Inorganic Chemistry

ARTICLE

pubs.acs.org/IC

High-Pressure Synthesis and Superconductivity of a New Binary Barium Germanide $BaGe_3$

Hiroshi Fukuoka,* Yusuke Tomomitsu, and Kei Inumaru

Department of Applied Chemistry, Faculty of Engineering, Hiroshima University, Higashi-Hiroshima 739-8527, Japan

Supporting Information

ABSTRACT: A new binary barium germanide $BaGe_3$ was prepared by high-pressure and high-temperature reactions using a Kawai type multi-anvil press. It crystallizes in a hexagonal unit cell with $a = 6.814(1)$ Å, $c = 5.027(8)$ Å, and $V = 202.2(5)$ Å^3 (the space group $P6_3/mmc$, No. 194). The unit cell contains two layers along the c axis composed of Ba atoms and Ge_3 triangular units. The triangular units stack along the c axis to form 1D columns in which the adjacent Ge_3 units turn to opposite directions. The columns, therefore, can be described as the face-sharing stacking of elongated Ge_6 octahedra. Each Ba atom is surrounded by six columns. $BaGe_3$ is metallic and shows superconductivity at 4.0 K. The band structure calculations revealed that there are four conduction bands mainly composed of Ge 4p and Ba 5d orbitals. From Fermi surface analysis, we confirmed that three of them have a large contribution of Ge 4pz orbitals in the vicinity of the Fermi level and show a simple 1D appearance. The remaining one contains Ge 4px, 4py, and Ba 5d contributions and shows a 2D property.

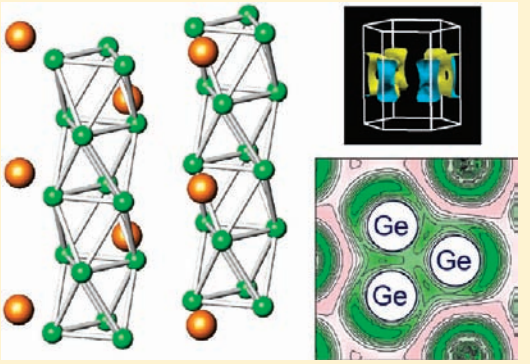

INTRODUCTION

The binary Ba−Ge system has received considerable attention in recent years because of its diversity of structure as well as interesting properties such as thermoelectric and superconducting behaviors. Figure 1 depicts the structural evolution with an increase in Ge content in the Ba−Ge binary system.[1,2] Binary compounds with Ge/Ba ≤ 2 form alloys or Zintl phases. The orthorhombic $BaGe_2$ containing Ge_4^{2-} anions is a typical example of the latter group and shows semiconducting properties.[3,4] The orthorhombic phase undergoes a phase transition at 4.0 GPa and 1000 °C to the α-$ThSi_2$ structure.[5] This high-pressure phase shows superconductivity with a critical temperature T_c of 4.93 K.[6]

In Ge-rich conditions, two clathrate compounds are produced under ambient pressure. They are $Ba_{24}Ge_{100}$ and Ba_8Ge_{43} having the type III and I clathrate structures, respectively.[7−14] The host Ge atoms compose 3D covalent networks with large cages where Ba atoms are situated. Recently, a new germanium clathrate compound, $BaGe_5$, has been reported.[15] It is a semiconducting Zintl phase.

These clathrate compounds and their derivatives prepared by substitution of post-transition elements for some Ge atoms are extensively studied as promising candidates for the application of thermoelectric devices.[9,16] The superconductivity of clathrate compounds also attracts much attention these days. $Ba_{24}Ge_{100}$ is isotypic with the superconducting silicon analogue $Ba_{24}Si_{100}$ and shows superconductivity at 0.24 K.[17−19] There have been many studies of the physical properties of $Ba_{24}Ge_{100}$.[20−23]

Thus, many binary compounds are reported in the Ba−Ge system. However, no 1:3 compound has been prepared, although many 1:3 compounds having the famous structure types of Cu_3Au, $BaPb_3$, Ni_3Sn, YGe_3, and so forth were discovered in many binary germanide systems. We have examined the reactions of 1:3 mixtures of Ba and Ge by changing reaction pressures from 5 to 13 GPa, and have successfully obtained a new binary barium germanide $BaGe_3$.

EXPERIMENTAL SECTION

$BaGe_3$ was prepared by the following two-step reactions. A mixture of Ba (Nakarai Tesque 99%) and Ge (Mitsuwa Pure Chemical 99.999%) with a molar ratio of 1:2 was reacted in an Ar-filled arc furnace to obtain $BaGe_2$. It was mixed with a Ge powder with a molar ratio $BaGe_2$/Ge = 1:1 (Ba/Ge = 1:3). The mixture was placed in an h-BN cell. The cell was placed in an MgO octahedral pressure medium and was heated at high pressures using a Kawai-type multi-anvil press.[24] We performed the reactions varying temperature (500−1200 °C) and pressure (3−13 GPa).

The products were characterized by X-ray powder diffraction (XRD) measurements with a Bruker AXS D8 Advance diffractometer with Ni-filtered CuKα radiation. The crystal structure was analyzed using a single crystal with a size of 0.05 × 0.10 × 0.10 mm^3. The X-ray diffraction data was collected using a Bruker APEX-II CCD diffractometer with graphite-monochromated MoKα radiation. The structure was solved and refined using the Bruker *SHELXTL* software package.[25] Chemical compositions of the products were examined by an electron probe micro-analyzer (EPMA) (JEOL JCMA-733). Magnetic susceptibility measurements were performed with a SQUID magnetometer (Quantum Design MPMS-5) in a 20 Oe field. Temperature dependence of electrical

Received: April 20, 2011
Published: June 06, 2011

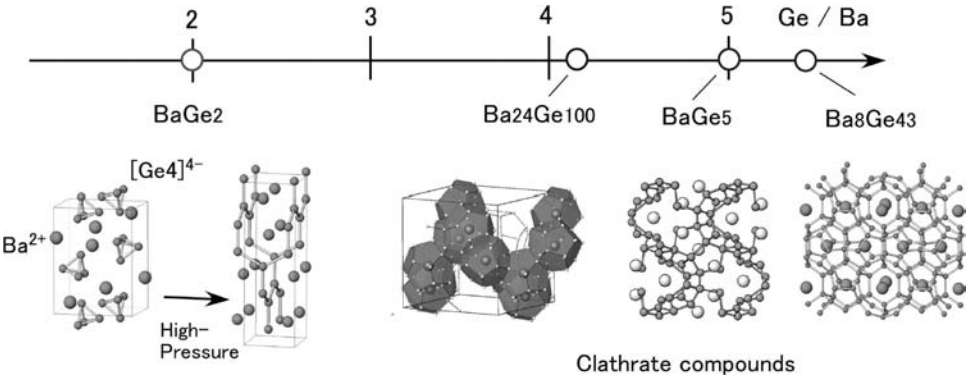

Figure 1. Binary compounds of the Ba−Ge system with a Ge to Ba ratio ranging from 2 to 6.

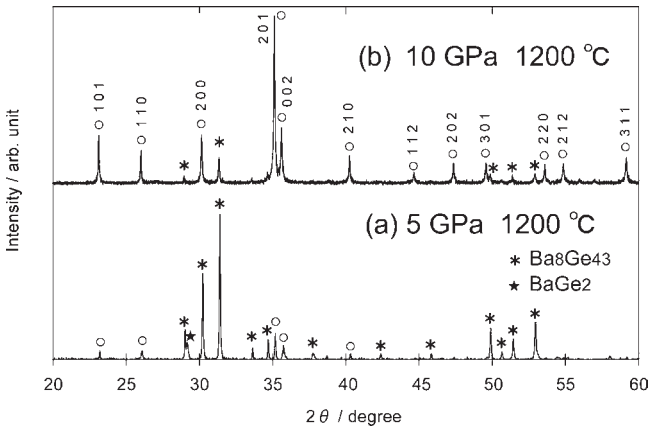

Figure 2. X-ray powder diffraction patterns of two samples prepared at 1200 °C under different pressures. Asterisk and star marks show the diffraction peaks of Type I clathrate compound and $BaGe_2$ (high-pressure phase), respectively. Open circles show diffractions of the new compound.

resistivity was observed with the van der Pauw method using dc from room temperature to 2 K.

The band structure calculation was performed using the WIEN2k package with a full-potential augmented plane-wave + local orbitals (APW+lo) code.[26,27] Some parameters used were as follows: Muffin-Tin radius (RMT), 4.0 for Ba and 2.46 for Ge; Gmax, 12; RMT × kmax, 7; number of k points, 10 000. Electron localization functional (ELF) and chemical bond analysis using Crystal orbital Hamilton population (COHP) techniques were calculated and analyzed using a tight-binding linear muffin-tin orbital-atomic sphere approximation with *TB-LMTO-ASA* software.[28]

RESULTS AND DISCUSSION

The reaction at 5 GPa and 1200 °C yielded Ba_8Ge_{43} and $BaGe_2$ with the α-$ThSi_2$ structure as shown in part a of Figure 2. Several peaks marked with open circles seemed to be attributed to a new phase. The new phase became a main product by the reaction at 10 GPa and 1200 °C. The XRD pattern shown in part b of Figure 2 could not be identified as any binary Ba−Ge compound.

We, therefore, performed single-crystal X-ray analysis and found that the phase crystallizes in a hexagonal unit cell with a = 6.814(1) Å, c = 5.027(8) Å, and V = 202.2(5) Å^3. The composition determined by the structure analysis was $BaGe_3$, which is identical to the composition $BaGe_{2.99}$ determined by the EPMA method. An EPMA image of $BaGe_3$ is shown in Figure S1 of the Supporting Information. The crystallographic data and atomic and thermal displacement parameters of $BaGe_3$ are listed in Tables 1 and 2.

Table 1. Crystallographic Data and Details on the Structure Determination of $BaGe_3$

formula	$BaGe_3$
fw	355.25
space group	$P6_3/mmc$ (No. 194)
a /Å	6.814(1)
c /Å	5.027(8)
V /Å^3	202.2(5)
Z	2
cryst size (mm)	0.05 × 0.1 × 0.1
diffractometer	Bruker APEX-II CCD
radiation (graphite monochromated)	MoKα
μ(Mo Kα)/mm^{-1}	31.261
2θ limit	53.88
No. of observed unique reflections	105
No. of variables	8
$R1$, $wR2$	0.0156, 0.0328
goodness of fit, S	1.239
largest diff. peak and hole	0.833/−0.525

The structure of $BaGe_3$ presented in Figure 3 is isotypic with the $BaSn_3$ structure.[29] It has a layer structure and each layer is composed of both Ba and Ge atoms. The arrangement of atoms in the layer is similar to that in a closest packing structure but not ideal. The Ge site is slightly away from the ideal position. This displacement forms Ge_3 triangular units with a Ge−Ge distance of 2.613(4) Å in the layers. The direction of apexes of the triangular units in adjacent layers is opposite. The triangular units, therefore, make elongated Ge_6 octahedra by sharing their faces and form 1D columns as shown in Figure 3. The Ge−Ge distance between the adjacent triangular units is 2.932(3) Å, which is quite longer than that of an intra-unit. Ba atoms are located around the columns. The physical properties of $BaGe_3$ possibly reflect this 1D nature of the structure.

Figure 4 shows the temperature dependence of the resistivity of $BaGe_3$. The resistivity decreases with decreasing temperature showing that $BaGe_3$ is metallic. Furthermore, the zero resistivity was observed below 4.0 K suggesting that $BaGe_3$ is a superconductor

dx.doi.org/10.1021/ic200826d |*Inorg. Chem.* 2011, 50, 6372–6377

Table 2. Atomic Coordinates and Thermal Displacement Parameters for $BaGe_3$[a]

atom	*x*	*y*	*z*	U_{11}	U_{22}	U_{33}	U_{12}	Ueq
Ba	2/3	1/3	1/4	0.0113(3)	$= U_{11}$	0.0160(3)	0.0056(1)	0.0129(2)
Ge	0.12783(5)	0.25567(9)	1/4	0.0132(3)	0.0120(3)	0.0182(4)	0.0060(2)	0.0195(4)

[a] All $U_{23} = U_{13} = 0$.

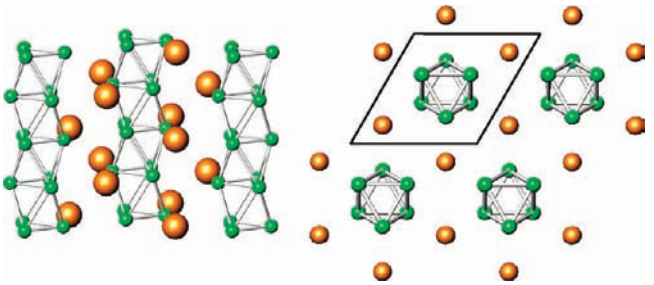

Figure 3. Crystal structure of $BaGe_3$ projected along the *c* axis (left) and on the *a*−*b* plane (right). Orange and green spheres show Ba and Ge atoms, respectively.

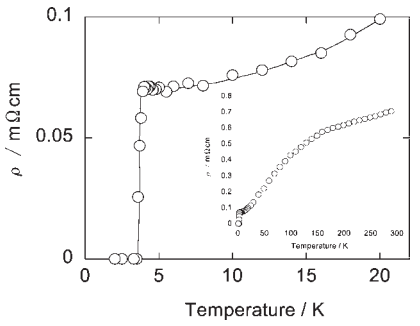

Figure 4. Temperature dependence of the electrical resistivity of $BaGe_3$.

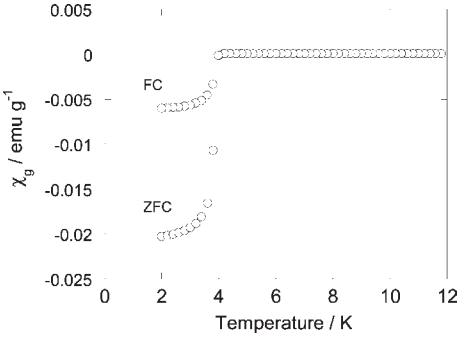

Figure 5. Temperature dependence of magnetic susceptibility of $BaGe_3$.

with the critical temperature (T_c) of 4.0 K. The magnetic susceptibility of $BaGe_3$ is presented in Figure 5. The Meissner effect was observed at 4.0 K and the superconducting volume fraction of the zero-field cooling sample at 2 K is calculated to be 146%. Owing to the demagnetization effect, the volume fraction is over 100%. From these observations, we confirmed that $BaGe_3$ is a new superconductor with a T_c of 4.0 K.

For further studies about the electronic properties of $BaGe_3$, we have performed the density of state (DOS) calculations. The

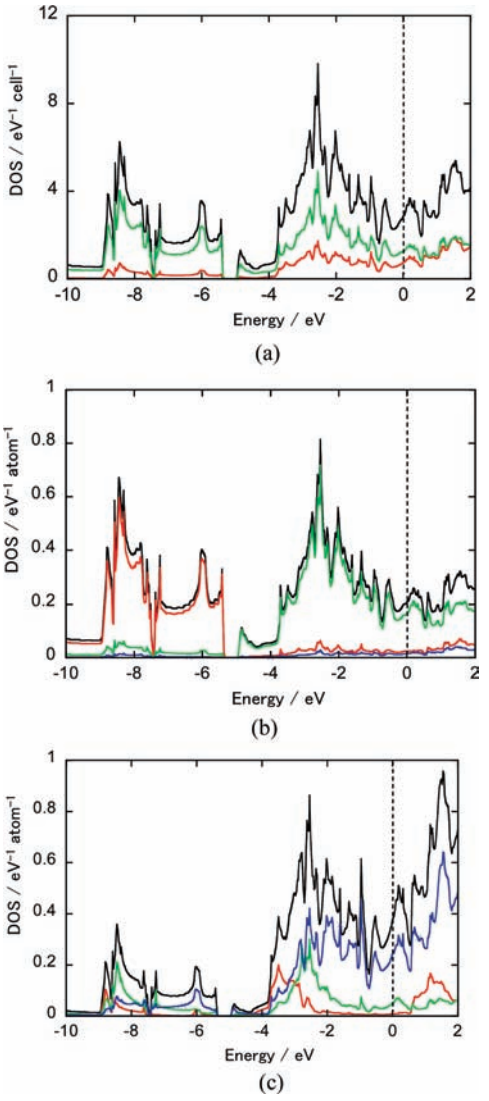

Figure 6. The density of state (DOS) of $BaGe_3$ obtained from APW+lo calculations (the *Wien2k* code). The Fermi level is set as zero. (a) Total DOS diagram. The black, green, and red plots are the total, Ge-total, and Ba-total DOSs, respectively. (b) Ge-partial DOS. The black, red, green, and blue lines show the total, 4s, 4p, and 4d contributions, respectively. (c) Ba-partial DOS. The black, red, green and blue lines show the contributions of the total, 5s, 5p, and 5d contributions, respectively.

results are shown in Figure 6. The total DOS diagram proves the metallic property of $BaGe_3$. The deep-lying bands below −5 eV are mainly composed of Ge 4s orbitals. The conduction bands are mainly composed of Ge 4p orbitals but a measurable contribution of Ba orbitals is also observed. The states in the vicinity of Fermi level (E_F) are mainly composed of Ge 4p and Ba 5d orbitals. It is noteworthy that the contribution of the Ge 4p*z*

dx.doi.org/10.1021/ic200826d |*Inorg. Chem.* 2011, 50, 6372–6377

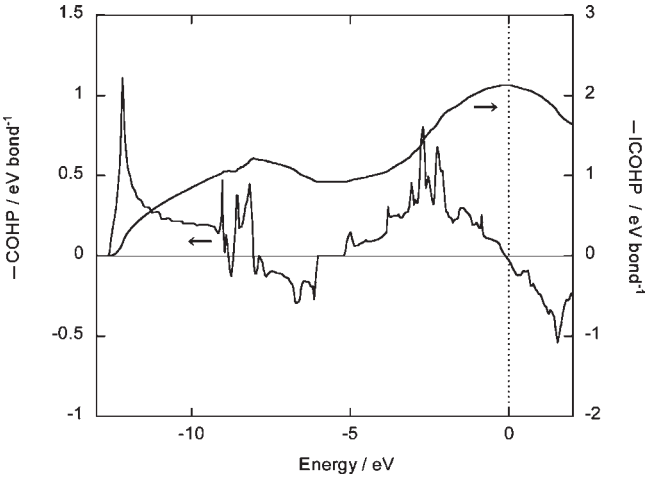

Figure 7. COHP and ICOHP diagrams of $BaGe_3$ for the Ge−Ge bond with a distance of 2.613 Å in the Ge_3 triangular unit.

orbital is observed to the conduction bands but large contributions of Ge 4p*x* and 4p*y* are also observed in the vicinity of E_F. This suggests that the two-dimensionally spread orbitals made of Ba 5d and Ge 4p orbitals are also important for the conductivity of $BaGe_3$ as well as the bands made of 1D Ge_3 columns. The detailed structure of conduction bands is discussed below using Fermi surface diagrams.

The COHP and ICOHP diagrams for the Ge−Ge bond with 2.613 Å in the Ge_3 triangular unit are helpful to understand the detailed electronic structure of the unit. They are shown in Figure 7. The −ICOHP values at the Fermi level is 2.1 eV/bond, clearly suggesting the presence of a strong Ge−Ge covalent bond.

A −ICOHP value of 0.78 eV/bond was obtained for the 2.932 Å Ge−Ge bond corresponding to the contact between two adjacent triangular units. This value also shows a fairly strong covalent interaction of Ge_3 triangles along the *c* axis, and supports the 1D column model of $BaGe_3$ from the point of view of electronic structure.

Figure 8 shows the electron localization functions for the $z = {}^1/_4$ plane of $BaGe_3$ projected along the *c* axis. Ba atoms and Ge_3 triangular units reside on the plane. At each corner of the triangular units, a crescent-shaped area with high ELF values (η = 0.7) is observed. This corresponds to a lone pair of electrons. Other elevations of ELF values (η = 0.6) are observed around the middle points between Ge atoms. They presumably show the covalent electrons of the Ge−Ge bonds. This is in good agreement with the results of the COHP analysis.

$LaGe_3$, $SrSn_3$, and $BaSn_3$ also contain Ge_3 or Sn_3 triangular units.[29−31] All of them are composed of layers including one part of guest atoms and three parts of tetrel atoms but the stacking manner of the layers is different. The layer sequence is ABAB··· or h in $BaGe_3$ and $BaSn_3$, whereas it is ABABCBCAC··· or hhc and ABABCACABCBC··· or hhcc in $LaGe_3$ and $SrSn_3$, respectively. Therefore, Ge_3 or Sn_3 units are one-dimensionally stacked in the former compounds but not in $LaGe_3$ and $SrSn_3$. Nonetheless, the ELF diagram of $BaGe_3$ is very similar to those of $LaGe_3$ and $SrSn_3$ as well as that of $BaSn_3$. The similarity shows the electronic structures of Ge_3 or Sn_3 triangular units in these compounds are quite similar to each other.

It is noteworthy to consider the schematic molecular orbitals (Figure 9) of Sn_3^{2-} proposed by Fässler et al.[29,31] They estimated the orbitals using cyclo-propanyl cations ($C_3R_3^+$) because it is

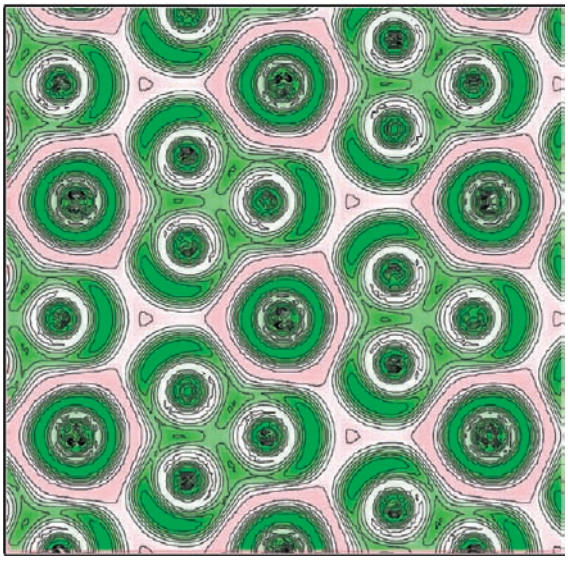

Figure 8. Electron localization function (ELF) diagram of $BaGe_3$ for the plane parallel to the *a*−*b* plane on which Ge_3 triangle units and Ba atoms are situated. Red and green colors show the low and high ELF areas, respectively.

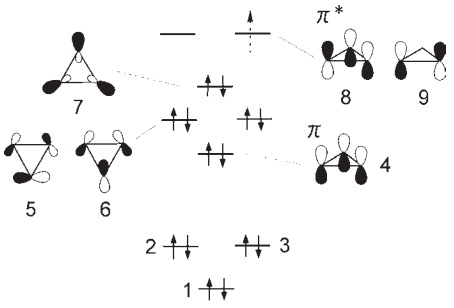

Figure 9. Schematic molecular orbitals of Sn_3^{2-} triangular unit proposed by Fässler et al. The highest occupied orbital for $BaGe_3$ is orbital 7. An arrow with dashed line shows the case of $LaGe_3$.

isoelectronic with Sn_3^{2-}. The Ge_3 unit probably has a similar electronic structure to that of Sn_3^{2-}. The lowest orbital (1) is a bonding one composed of three Sn 5s orbitals. The second lowest ones (2, 3) are 5s antibonding orbitals. These are well corresponding to the COHP diagram for $BaGe_3$ in Figure 7. The bands between −14 to −8 eV in the COHP diagram have negative COHP values, whereas positive values are seen from −8 to −6 eV. The former would be assigned to bonding bands of Ge 4s orbitals and the latter to antibonding ones.

The bands ranging −4 eV to E_F have negative COHP values, bonding character. They correspond to the four occupied orbitals (4 − 7) in Figure 9. They can be assigned to a π-bonding orbital and three lone pairs of the Ge_3 unit. The highest occupied orbital (HOMO) of $BaGe_3$ is orbital 7, which has a bonding character. In $LaGe_3$, however, one more electron should be accommodated in the Ge_3 unit because one La atom donates three electrons. The additional electrons occupy π^* orbitals (8, 9). This should weaken the covalency of the Ge−Ge bond in the Ge_3 unit. In fact, the Ge−Ge distance is 2.634 Å for $LaGe_3$, which is longer than that for $BaGe_3$ (2.613 Å).[30] Thus, the consideration about the electronic structure of the Ge_3 unit is possible from the

dx.doi.org/10.1021/ic200826d |*Inorg. Chem.* 2011, 50, 6372–6377

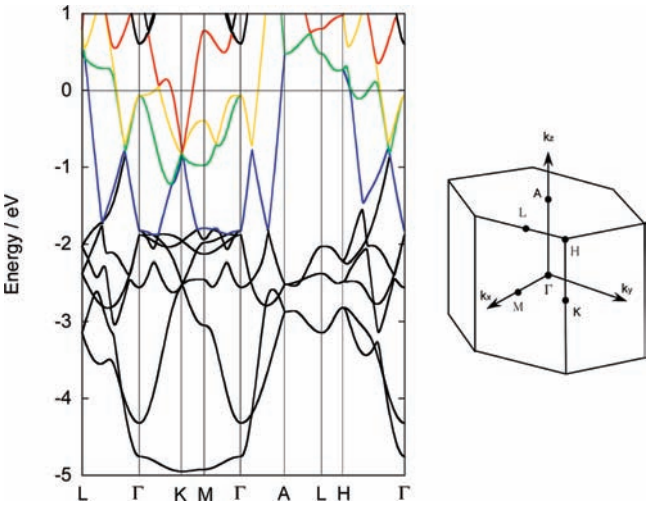

Figure 10. Band structure (k-dispersion) of $BaGe_3$ and its schematic Brillouin zone with the reciprocal repetition axes. Blue, green, yellow, and red bands correspond to the Fermi surfaces of bands 51, 52, 53, and 54 in Figure 12, respectively.

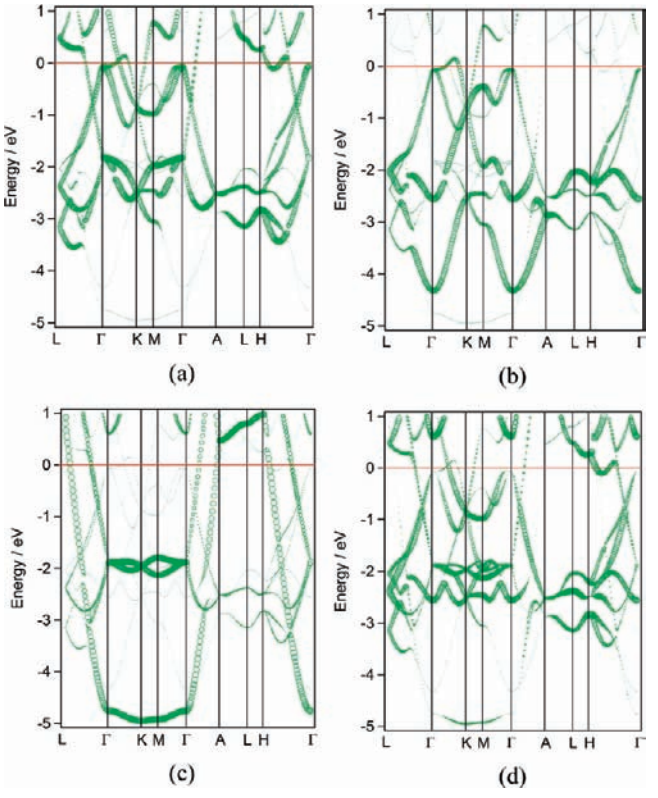

Figure 11. Contributions of the (a) Ge p*x*, (b) Ge p*y*, (c) Ge p*z*, and (d) Ba d orbitals are shown in a fat band presentation.

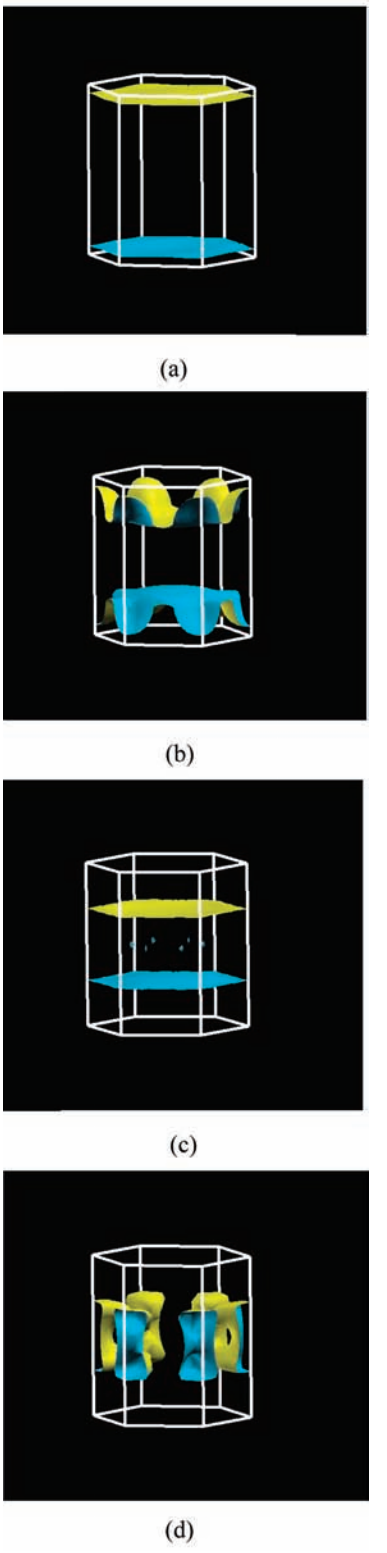

Figure 12. Fermi surfaces of $BaGe_3$ calculated with *Wien2k* and *XCrysDen*[32] software; (a) band 51, (b) band 52, (c) band 53, and (d) band 54.

discussion based on this simple model. Of course, because theoretical calculations should be required for detailed research for the electronic structure, we calculated the band structure of $BaGe_3$ using *Wien2k* and *TB-LMTO-ASA* programs.

The band structure of $BaGe_3$ along the highly symmetrical paths is shown in Figure 10. Three bands (51, 52, and 53; latter two are degenerated) cross the E_F along the path from Γ to A, corresponding the direction of the *c* axis in the real space. According to the fat band analysis, these bands are mainly contributed by Ge 4p*z* orbitals in the vicinity of E_F as shown in part c of Figure 11. The Fermi surfaces of these bands are

dx.doi.org/10.1021/ic200826d |*Inorg. Chem.* 2011, 50, 6372–6377

presented in parts a, b, and c of Figure 12. The surfaces show a typical 1D character. These bands, therefore, reflect the column structure of Ge_3 triangular units. Another band (54) crosses the E_F along the Γ to K and K to M. The Fermi surface of the band 54 (part d of Figure 12) shows an electron-like surface. This band is mainly composed of Ge 4p*x*, 4p*y*, and Ba 5d orbitals as shown in parts a, b, and d of Figure 11, respectively. Because of the combination of Ge and Ba orbitals, $BaGe_3$ acquires the conduction path spreading in the *a*−*b* plane.

If the electronic structure of $BaGe_3$ were highly 1D, the crystal structure would have a superstructure along the *c* axis due to a presence of charge density wave (CDW). The 2D interactions between Ba and Ge would prevent the CDW and help the occurrence of superconductivity of $BaGe_3$.

CONCLUSIONS

We prepared a new binary trigermanide $BaGe_3$ by high-pressure and high-temperature reactions. It crystallizes in the $BaSn_3$ structure ($P6_3/mmc$) containing Ge_3 triangular units. The units stack along the *c* axis and form 1D $[Ge_3]_\infty$ columns. The COHP and ELF calculations revealed the electronic structure of the Ge_3 triangular unit. Each Ge atom has a lone pair and a strong covalent bond is observed between the Ge atoms. $BaGe_3$ shows a superconducting transition at 4.0 K. There are four conduction bands; three have 1D character and are mainly contributed by Ge 4p*z* orbitals in the vicinity of E_F; the remaining one shows an electron-like Fermi surface contributed by Ge 4p*x*, 4p*y*, and Ba 5d orbitals.

ASSOCIATED CONTENT

Supporting Information. EPMA image of $BaGe_3$, and the crystallographic information file (CIF). This material is available free of charge via the Internet at http://pubs.acs.org.

AUTHOR INFORMATION

Corresponding Author

*Phone: +81-824-24-7742. Fax: +81-824-24-5494. E-mail: hfukuoka@hiroshima-u.ac.jp.

ACKNOWLEDGMENT

We are grateful to Mr. Yasuhiro Shibata of Hiroshima University for his help with the EPMA measurements. This work was supported by a Grant-in-Aid for Scientific Research from the Ministry of Education, Science, and Culture of Japan, Grant No. 16037212, 16750174, 18750182, 18027010, and 20550178.

REFERENCES

(1) Pani, M.; Palenzona, A. *J. Alloys Compd.* **2008**, *462*, L9–11.
(2) Carrillo-Cabrera, W.; Borrmann, H.; Paschen, S.; Baenitz, M.; Steglich, F.; Grin, Y. *J. Solid State Chem.* **2005**, *178*, 715–728.
(3) Betz, A.; Schafer, H.; Weiss, A.; Wulf, R. *Z. Naturforsch., B: Chem. Sci.* **1968**, *23*, 878.
(4) Vaughey, J. T.; Miller, G. J.; Gravelle, S.; Leon-Escamilla, E. A.; Corbett, J. D. *J. Solid State Chem.* **1997**, *133*, 501–507.
(5) Evers, J.; Oehlinger, G.; Weiss, A. *J. Less-Common Met.* **1980**, *69*, 399–402.
(6) Evers, J.; Oehlinger, G.; Ott, H. R. *J. Less-Common Met.* **1980**, *69*, 389–391.
(7) Fukuoka, H.; Iwai, K.; Yamanaka, S.; Abe, H.; Yoza, K.; Haming, L. *J. Solid State Chem.* **2000**, *151*, 117–121.
(8) Carrillo-Cabrera, W.; Curda, J.; Paschen, S.; von Schnering, H. G. *Z. Kristallogr.—New Cryst. Struct.* **2000**, *215*, 207.
(9) Kim, S.-J.; Hu, S.; Uher, C.; Hogan, T.; Huang, B.; Corbett, J. D.; Kanatzidis, M. G. *J. Solid State Chem.* **2000**, *153*, 321–329.
(10) Petkova, V.; Vogt, T. *Solid State Commun.* **2003**, *127*, 43–46.
(11) Carrillo-Cabrera, W.; Curda, J.; Peters, K.; Paschen, S.; Baenitz, M.; Grin, Y.; von Schnering., H. G. *Z. Kristallogr.—New Cryst. Struct.* **2000**, *215*, 321–322.
(12) Aydemir, U.; Candolfi, C.; Borrmann, H.; Baitinger, M.; Ormeci, A.; Carrillo-Cabrera, W.; Chubilleau, C.; Lenoir, B.; Dauscher, A.; Oeshler, N.; Steglich, F.; Grin, Y. *Dalton Trans.* **2010**, *39*, 1078–1088.
(13) Fukuoka, H.; Kiyoto, J.; Yamanaka, S. *J. Solid State Chem.* **2003**, *175*, 237–244.
(14) Carrillo-Cabrera, W.; Budnyk, S.; Prots, Y.; Grin, Y. *Z. Anorg. Allg. Chem.* **2004**, *630*, 2267–2276.
(15) Aydemir, U.; Akselrud, L.; Carrillo-Cabrera, W.; Candolfi, C.; Oeschler, N.; Baitinger, M.; Steglich, F.; Grin, Y. *J. Am. Chem. Soc.* **2010**, *132*, 10984–10985.
(16) Paschen, S.; Tran, V. H.; Baenitz, M.; Carrillo-Cabrera, W.; Grin, Y.; Steglich, F. *Phys. Rev.* **2002**, *B65*, 134435.
(17) Fukuoka, H.; Ueno, K.; Yamanaka, S. *J. Organomet. Chem.* **2000**, *611*, 543–546.
(18) Grosche, F. M.; Yuan, H. Q.; Carrillo-Cabrera, W.; Paschen, S.; Langhammer, C.; Kromer, F.; Sparn, G.; Baenitz, M.; Grin, Y.; Steglich, F. *Phys. Rev. Lett.* **2001**, *87*, 247003.
(19) Yuan, H. Q.; Grosche, F. M.; Carrillo-Cabrera, W; Pacheco, V; Sparn, G; Baenitz, M; Schwarz, U; Grin, Y; Steglich, F. *Phys. Rev.* **2004**, *B70*, 174512.
(20) Kanetake, F.; Harada, A.; Mukuda, H.; Kitaoka, Y.; Rachi, T.; Tanigaki, K.; Itoh, K.; Haller, E. E. *J. Phys. Soc. Jpn.* **2009**, *78*, 104710.
(21) Shimizu, H.; Fukushima, T.; Kume, T.; Sasaki, S.; Fukuoka, H.; Yamanaka, S. *J. Appl. Phys.* **2007**, *101*, 113531.
(22) Rachi, T.; Kitajima, M.; Kobayashi, K.; Guo, F. Z.; Nakano, T.; Ikemoto, Y.; Kobayashi, K.; Tanigaki, K. *J. Chem. Phys.* **2005**, *123*, 074503.
(23) Tang, J.; Xu, J.; Heguri, S.; Fukuoka, H.; Yamanaka, S.; Akai, K.; Tanigaki, K. *Phys. Rev. Lett.* **2010**, *105*, 176402.
(24) Fukuoka, H. *Rev. High Press. Sci. Technol.* **2006**, *16*, 329–335.
(25) *SHELXS-97*; Sheldrick, G. University of Göttingen: Germany, 1997.
(26) Blaha, P.; Schwarz, K.; Sorantin, P.; Trickey, S. B. *Comput. Phys. Commun.* **1990**, *59*, 399.
(27) Blaha, P.; Schwarz, K.; Madesen, G. K. H.; Kvasnicka, D.; Luitz, J. *Wien2k*, An Augmented Plane Wave + Local Orbitals Program for Calculating Crystal Properties; Karlheinz Schwarz, Techn. Universität Wien: Austria, 2001.
(28) Jepsen, O.; Burkhardt, A.; Andersen, O. K. The Program *TBLMTO*, version 4.7; Max Planck Institute für Festkörperforschung: Stuttgart, 1999.
(29) Fässler, T. F.; Kronseder, C. *Angew. Chem., Int. Ed. Engl.* **1997**, *36*, 2683–2686.
(30) Fukuoka, H.; Suekuni, K.; Onimaru, T.; Inumaru, K. *Inorg. Chem.* **2011**, *50*, 3901–3906.
(31) Fässler, T. F.; Hoffmann, S. *Z. Anorg. Allg. Chem.* **2000**, *626*, 106–112.
(32) Kokalj, A. *Comput. Mater. Sci.* **2003**, *28*, 155.